Applied Surface Science 637 (2023) 157837

Contents lists available at ScienceDirect

Applied Surface Science

journal homepage: www.elsevier.com/locate/apsusc

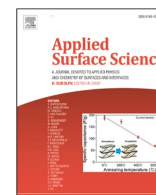

Full Length Article

Alteration and interrogation of ultra-thin layer of silicon by reactive molecular ion implantation

Joy Mukherjee [a], Sudip Bhowmick [a], Sabyasachi Karmakar [b], Dipak Bhowmik [a], Biswarup Satpati [b], Satyajit Hazra [b], Prasanta Karmakar [a,*]

[a] *Ion Beam Development and Application Section, RIB Group, Variable Energy Cyclotron Centre, HBNI, 1/AF Bidhannagar, Kolkata 700064, India*
[b] *Saha Institute of Nuclear Physics, HBNI, 1/AF Bidhannagar, Kolkata 700064, India*

ARTICLE INFO

Keywords:
Reactive molecular ion beam
Ultrathin silicon compounds
XPS
XRR
UV–VIS
Multiple bandgap

ABSTRACT

We report the engineering of ultrathin top layer of Si substrate by low energy (14 keV) reactive ion bombardment. The physicochemical nature of the layer is interrogated and the optical properties are explored. Irradiation of nitric oxide (NO^+) and mixture of carbon monoxide & nitrogen ($CO^+ + N_2^+$) ions on Si surface at normal incidence leads to formation of multiple chemical phases of Si with varying ion distribution within the layer. It is found that the chemistry of the topmost layer (~5 nm) is massively modified by the reactive projectiles, while implanted rich layer is formed at a depth of 25 to 37 nm followed by an intermediate amorphous Si layer of 20 nm thickness. The Ultra Violet-Infrared (UV-IR) response of the modified layer reveals high sensitivity in the UV region. The change in optical bandgap, estimated from Kubelka-Munks theory, indicates the presence of multiple direct and indirect bandgaps. The potential applications of such chemically modified multi-layered ultra-thin Si are addressed here.

1. Introduction

Silicon oxide, silicon carbide, silicon nitride and silicon oxy-nitride thin films are used for the development of electronic and optoelectronic devices, bio sensors, low dielectric materials, and nano-mechanical components due to their appropriate electronic, chemical, thermal, and mechanical properties [1–8]. Now a day, such ultrathin layers have tremendous application in ultra-thin silicon nitride/oxide solar cell, advance MOSFET, resonant tunnel diode etc. [9–12]. Synthesis of these films are, usually, carried out by plasma enhanced chemical vapor deposition [13,14], magnetron sputtering, and other film deposition techniques. In these processes, the control on concertation and film thickness is not easy, and the films are not contamination free. As an alternative process, the low energy ion implantation serves several purposes of ultrathin films synthesis. It ensures the precise control in thickness, concentration and contamination [15,16]. Further, the implantation of single ion species can synthesize single chemical compound on the surface [17], while molecular (NO^+ and ($CO^+ + N_2^+$)) ions can form multiple chemical phases due to simultaneous bombardment of multiple projectile ion on the surface[17–19]. However, studies of ion beam induced chemical modification of ultrathin Si layer are rare, specifically, molecular beam induced simultaneous development of multiple chemical phases by normal incidence ion bombardment is new and challenging. Moreover, for applications of such layer, basic understanding of chemical phase formation and optical nature of the ultrathin films need to be well studied.

This manuscript investigates the formation of ultrathin layer with multiple chemical phases due to 14 keV nitric oxide (NO^+), and ($CO^+ + N_2^+$) ion bombardment on Si substrate at normal incidence. The developed chemical phases due to irradiation of these ions are detected by X-ray photoelectron spectroscopy. The variation of electron density as a function of depth is investigated using X-ray reflectivity measurement. Further, the modified layer is investigated by high-resolution cross-sectional transmission electron microscopy (TEM). The investigations reveal that the modified layer is approximately 40 nm thick and consists of three sublayers. The top most 5 nm region is highly altered by the reaction of projectile ions with Si atoms, while second layer is mostly amorphous Si and the third sublayer is enriched with the implanted ion species. The chemically altered top layer is evident from the surface sensitive XPS measurements, while the inner sublayers are interrogated by XRR and TEM. The profiles of damage and implantation as a function of depth are also estimated by Monte Carlo SRIM

* Corresponding author.
E-mail address: prasantak@vecc.gov.in (P. Karmakar).

https://doi.org/10.1016/j.apsusc.2023.157837
Received 3 February 2023; Received in revised form 16 June 2023; Accepted 19 June 2023
Available online 23 June 2023
0169-4332/© 2023 Elsevier B.V. All rights reserved.

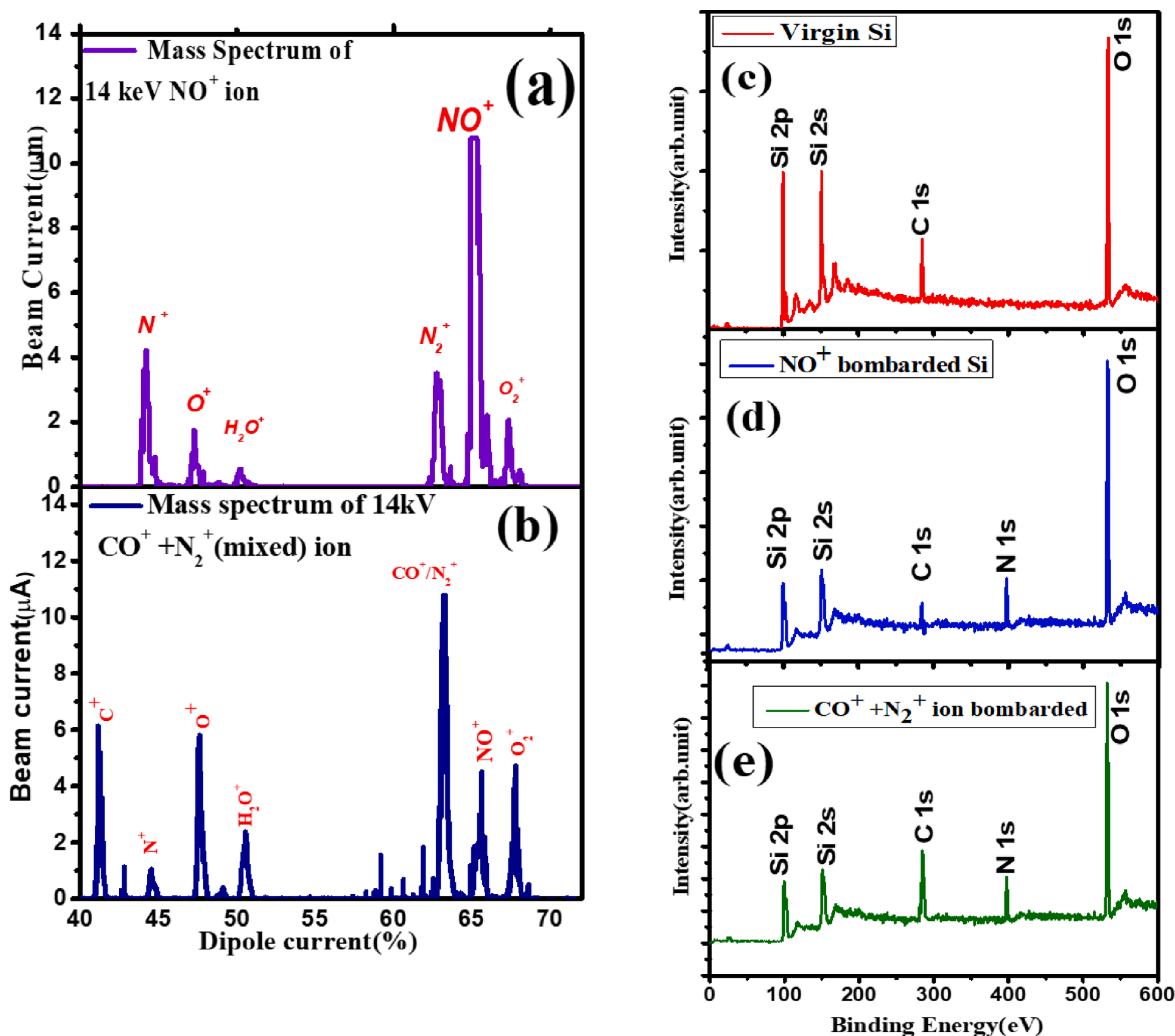

Fig. 1. Mass spectrum of (a) Hetero nuclei (NO^+) & (b) ($CO^+ + N_2^+$) ion extraction. XPS survey scan of (c) virgin (d) NO^+ (e) ($CO^+ + N_2^+$) ion bombarded Si surfaces.

simulation [20], which is consistent with the experimental results. The UV-IR reflectivity is used to study the variation of refractive index of the physico-chemically altered and layered films over the entire UV-IR region. The change in bandgap due to presence of several chemical phases is also marked in this article.

2. Experimental

Commercially available p-type single crystal (1 0 0) silicon wafers of size 1 cm × 1 cm are used for irradiation after proper cleaning with trichloroethylene in an ultrasonic bath. The ions are produced in an all-permanent magnet based 2.4 GHz Electron Cyclotron Resonance (ECR) ion source, which consists of a plasma chamber, permanent magnets, microwave source and gas feeding system. The magnets provide an axial and radial magnetic field to gyrate the electrons at cyclotron frequency of 2.4 GHz and confine within a specific region of the plasma chamber. Gas of which ions are to be produced is injected into the plasma chamber. When the microwave power of same frequency (2.4 GHz) is transported to the plasma chamber through a wave guide, the power is resonantly transferred to the electrons. The energetic electrons ionize the gas and form the ECR plasma. The ions are extracted from the plasma through an aperture by applying appropriate electric field. In order to generate NO^+ ions, nitrogen and oxygen gases are introduced in equal partial pressure into the ion source. The base pressure of the ECR chamber is 5×10^{-7} mbar. Similarly, carbon dioxide, and nitrogen gases are introduced into the ECR ion source to produce ($CO^+ + N_2^+$) ions. The ion with different mass to charge(A/q) ratio are filtered using a dipole electromagnet. Interestingly, carbon monoxide and molecular nitrogen ions with same mass to charge ratio (A/q = 28) are filtered out at same magnetic field and used as ($CO^+ + N_2^+$) ion beam. Finally, the ions are implanted on Si surface at the target chamber. The pressure of the target chamber is 9×10^{-8} mbar throughout the experiment.

The surface chemical composition before and after ion bombardment is detected using Omicron multi probe X-ray photoelectron spectrometer (XPS) in ultra-high vacuum ($\sim 10^{-8}$ mbar), equipped with monochromatic photon energy 1486.6 eV (Al K_α) and EA 125 hemispherical analyzer [21]. The energy resolution of the analyzer is 0.6 eV. The binding energy is calibrated by assuming the peak position of C 1 s at 284 eV [22]. The corresponding XPS spectra are fitted by casa peak fit software using Gaussian –Lorentzian(GL) distribution with the help of ML algorithm [23]. No constraints are applied during fitting.

The X-ray reflectivity measurements of the ion modified samples are carried out using an X-ray diffractometer (Smartlab, Rigaku) equipped with a copper source (wavelength 1.54 Å) [24]. The scattered beam is detected using NaI scintillation detector. Data is recorded in such a condition that the incident angle is equal to the reflected angle and both

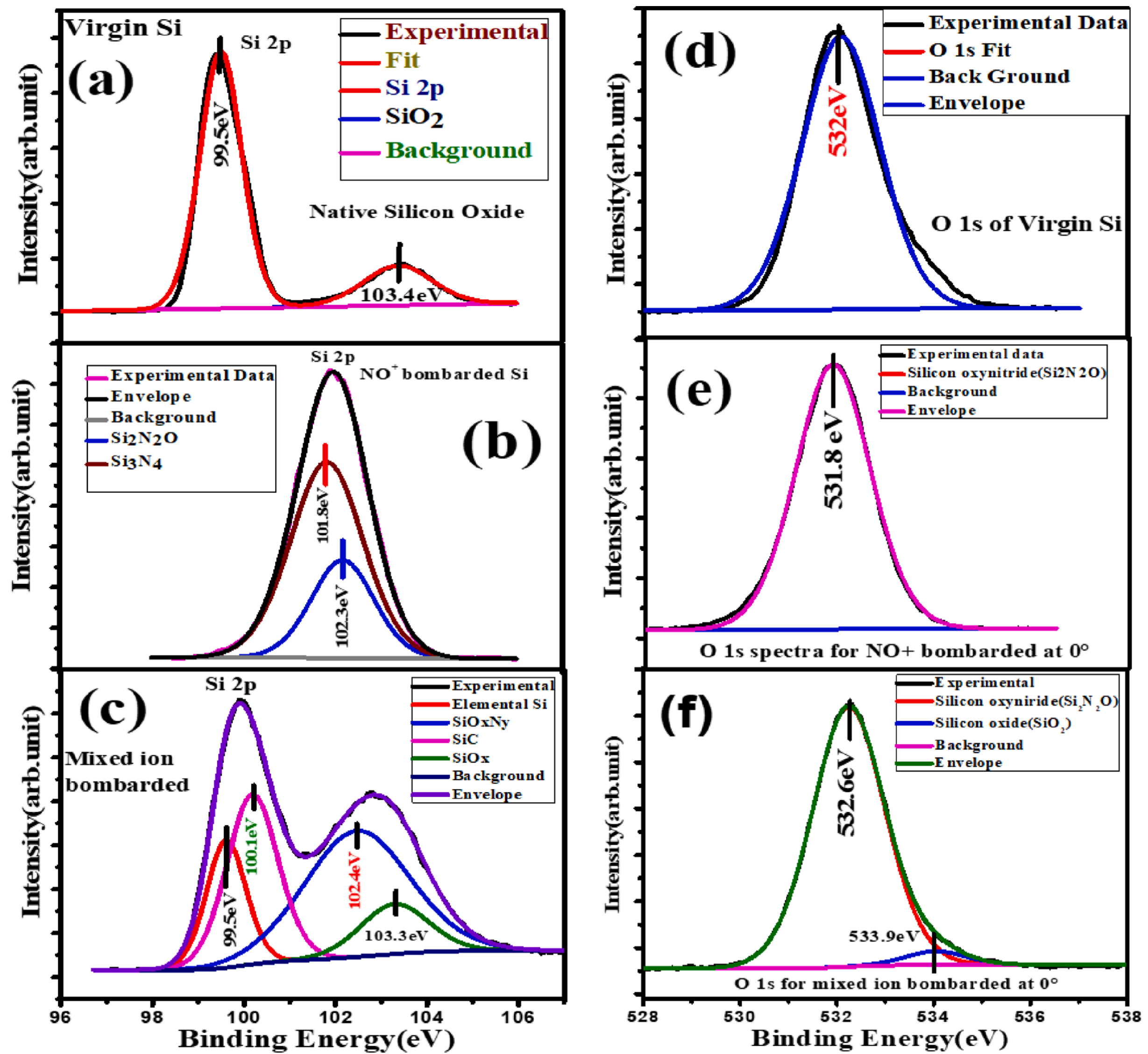

Fig. 2. High Resolution X-Ray Photoelectron Spectra of Si 2p of (a)Virgin Si, (b)NO^+ bombarded Si, (c) CO^+ +N_2^+ bombarded Si & O 1 s of (d) Virgin Si, (e) NO^+ bombarded Si, (f) CO^+ + N_2^+ bombarded Si at 0° ion incidence with fluence 1 × 10^{18} ions/cm^2.

are in a scattering plane. Under this condition, the resolution of the non-vanishing wave-vector q_z (=4π SinΘ/λ) is 0.0014 $Å^{-1}$.

The cross-sectional Transmission Electron Microscope study is carried using FEI, Tecnai G2 F30, S-Twin microscope operating at 300 kV with a Gatan imaging filter (mode 963). The sample is prepared by mechanical grinding, dimpling and ion polishing for TEM study. The optical response by means of UV-IR reflectivity of pristine and ion modified surfaces are recorded using Shimadzu 3600 UV-IR spectrometer ranging from 190 nm to 1200 nm. This reflectivity data is used to estimate the variation of refractive index as well as optical bandgap of the newly developed material.

3. Results and discussions

The mass spectra of projectile ions and the XPS survey spectra of the Si samples before and after ion irradiation are shown in Fig. 1. The most intense peak corresponds to NO^+ ion is depicted in Fig. 1(a). Similarly, the intense peak of (CO^++N_2^+) ion is shown in Fig. 1(b). Since, the mass to charge ratio (A/q) of CO^+ and N_2^+ are same (28:1), they are filtered at same magnetic field of the dipole electromagnet (Fig. 1(b)). The elements present in Si surface before and after the ion bombardment (fluence 1 × 10^{18} ions/cm^2) are identified from the XPS survey scans, and presented in Fig. 1(c)-(e). The presence of nitrogen is detected after NO^+ ion bombardment (Fig. 1(d)), whereas the (CO^++N_2^+) ion bombardment leads to change in the intensity of carbon, oxygen and nitrogen compared to virgin Si surface. Trace amount of carbon contamination is found in virgin Si due to wafer processing.

In order to investigate the surface chemical nature of virgin and ion modified Si surface, the high-resolution XPS spectra are presented in Fig. 2. The high resolution Si 2p spectra of virgin Si (Fig. 2(a)) is best fitted by two GL peaks (GL-30) positioned at 99.5 eV and 103.4 eV, corresponding to elemental Si and native silicon oxide (SiO_2) [25]. The formation of native oxide is due to the exposure of sample in air before experiment. The high-resolution Si 2p of NO^+ bombarded Si at angle 0° with fluence 1 × 10^{18} ions/cm^2 (Fig. 2(b)) shows a broad spectrum centered at 102 eV. This wide spectrum is fitted in two peaks (GL −30) positioned at 101.8 eV and 102.3 eV, confirming the formation of silicon nitride [26] and silicon oxynitride [27], respectively. Similarly, the high-resolution Si 2p spectrum of (CO^+ + N_2^+) ion bombarded Si with same ion energy, fluence and incidence angle is presented in Fig. 2(c). The broad Si 2p peak is fitted in four GL peaks at 99.5 eV, 100.1 eV, 102.4 eV and 103.3 eV, which indicate the presence of elemental Si and

Table1
Atomic percentage of Si in virgin and ion bombarded Si surfaces.

Sample	Atomic % of Elemental Si	Atomic % of Si in form of SiC	Atomic % of Si in form of Si_3N_4	Atomic % of Si in form of SiOx/ SiO_2	Atomic % of Si in form of SiO_xN_y
Virgin Si	81			19	
NO^+ bombarded	31		27		42
$CO^+ + N_2^+$ bombarded	18	28		10	44

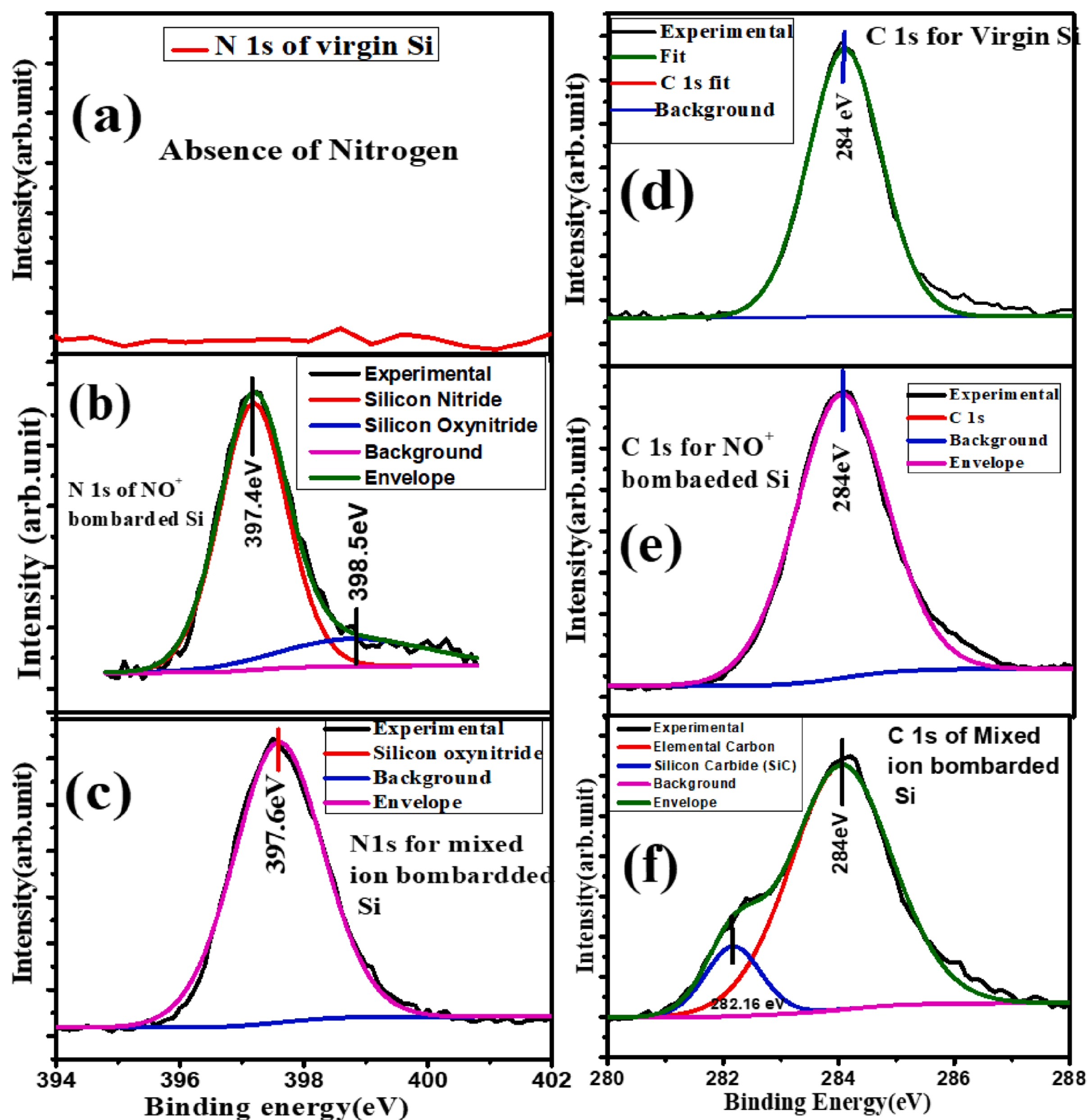

Fig. 3. High resolution X-ray Photoelectron spectroscopy of N 1 s of (a) virgin Si, (b) NO^+ bombarded Si, (c) $CO^+ + N_2^+$ bombarded Si. C 1 s spectrum of (d) virgin Si, (e), NO^+ bombarded Si, (f) $CO^+ + N_2^+$ bombarded Si at 0° ion incidence with fluence 1×10^{18} ions/cm^2.

formation of silicon carbide [28], silicon oxynitride [27] and silicon oxide [29], respectively. Hence, the chemical shift of Si 2p of ion modified surfaces indicate the presence of multiple chemical phases in case of molecular (NO^+) and ($CO^+ + N_2^+$) ion bombardment on Si surface. The atomic percent of Si in the form of element and its compounds is estimated from the high-resolution Si 2p spectra and are listed in Table 1. The average depth of information for the XPS measurements is approximately 5 nm. Thus, the information obtained from the XPS is restricted within the surface region. Further, the samples are not homogeneous along the depth because of native oxide formation in virgin Si and reactive ion implantation in irradiated Si samples. For virgin Si, native oxide layer is approximately 1.5 nm thick. The native oxide layer is also not homogeneous along the depth. The oxidation is maximum at the surface and decrease with the depth. We, thus, observed 19 and 81 atomic percent of Si in oxide and elemental states respectively, in the virgin Si sample. In case of NO^+ and ($CO^+ + N_2^+$) bombarded Si, the

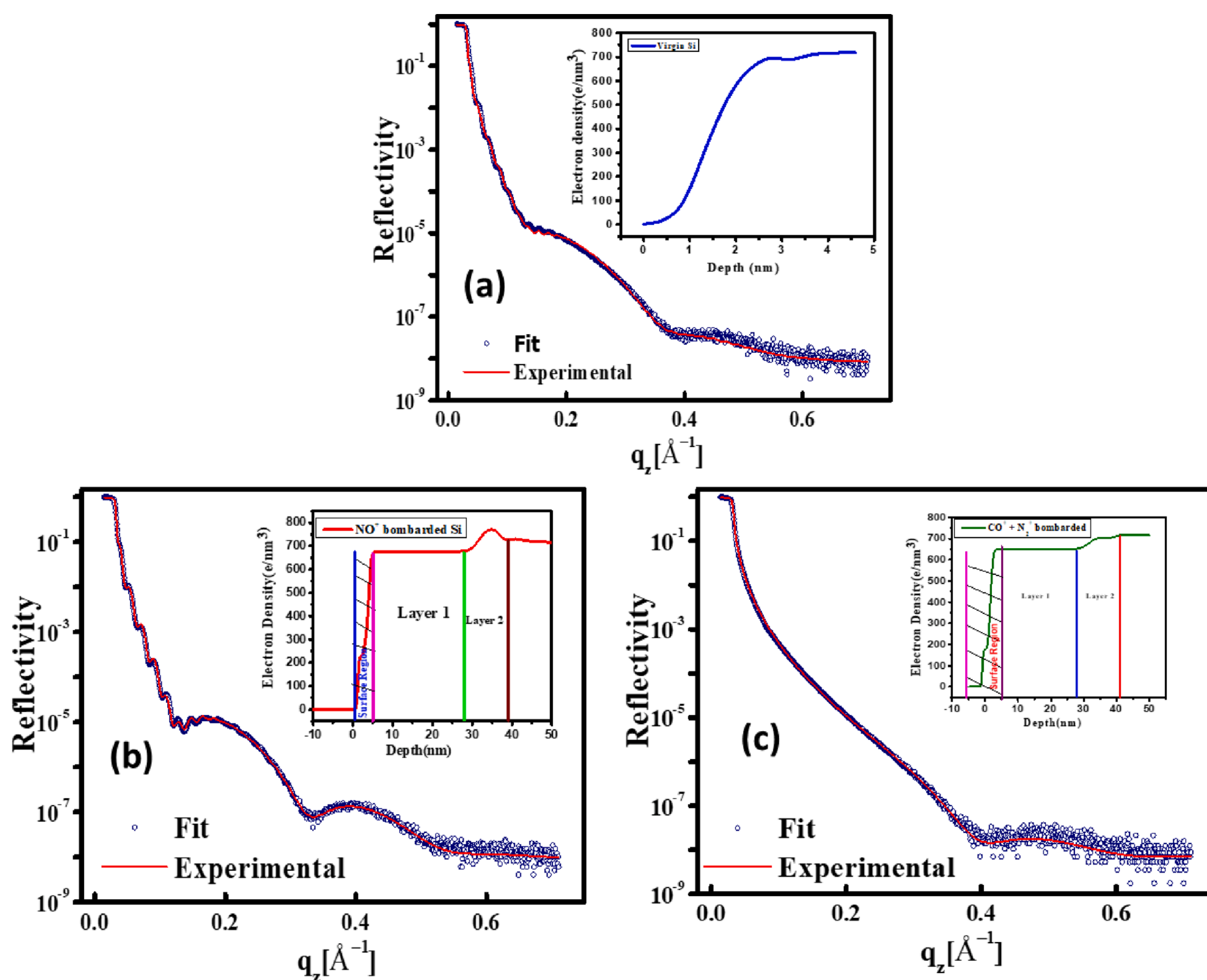

Fig. 4. X-ray Refelectivity of (a) virgin Si, (b) NO^+ bombarded Si, (c) ($CO^+ + N_2^+$) ion bombarded Si. Variation of corresponding electron density profile with depth are plotted in inset.

modified layer thickness is much more than the XPS information depth. Therefore, the data shown in Table 1 provides the information up to the depth (~5 nm) of information only. It is observed that 31% and 18% of Si atoms are in elemental form for NO^+ and ($CO^+ + N_2^+$) bombarded Si, respectively, while rest of the Si atoms form compounds as shown in Table 1. As we used uniform broad ion beam, we assumed all the samples are homogeneous in lateral direction; however, concentration and nature vary along the depth that has been probed by XRR and cross-sectional TEM (described later).

Further, to ensure the formation of these chemical compounds, corresponding high resolution spectra of individual elements i.e., O1s, N1s and C 1 s are also presented in Figs. 2 and 3. The high resolution O 1 s spectrum of virgin Si (Fig. 2(d)) with a peak positioned at 532 eV confirms the presence of native silicon oxide [30]. The chemical shift of high resolution O 1 s spectrum (Fig. 2(e)) of NO^+ bombarded Si towards lower binding energy (531.8 eV) ensures the formation of silicon oxynitride [31]. The O 1 s spectrum of ($CO^+ + N_2^+$) ion bombarded Si (Fig. 2 (f)) is fitted in two GL peaks at 532.6 eV and 533.9 eV confirming the presence of silicon oxynitride [31] and silicon oxide [32].

The absence of nitrogen in virgin Si is obvious from Fig. 1(b) and 3 (a), with no distinct peak around 397 eV. The high resolution N 1 s spectrum of NO^+ ion bombarded Si (Fig. 3(b)) is fitted with two GL peaks positioned at 397.4 eV and 398.5 eV corresponding to silicon oxynitride [33] and silicon nitride, respectively [34]. Similarly, N 1 s peak at 397.6 eV(Fig. 3(c) indicates the existence of silicon oxynitride [31] for ($CO^+ + N_2^+$) bombardment. The presence of elemental carbon in virgin Si is detected from the C 1 s peak at 284 eV (Fig. 3(d)). C 1 s spectrum of NO^+ ion bombarded Si (Fig. 3(e)) also shows the elemental form of the impurity carbon, but C 1 s spectrum of ($CO^+ + N_2^+$) ion bombarded Si indicates silicon carbide (282.16 eV) formation in addition to the elemental carbon (284 eV)[35] (Fig. 3(f)). Therefore, in case of NO^+ bombardment, silicon oxynitride and silicon nitride phases are formed while a mixture of silicon carbide, silicon oxynitride and silicon oxide is formed due to ($CO^+ + N_2^+$) ion bombardment.

Therefore, the detailed XPS analysis clarifies that normal bombardment of NO^+ on Si surface leads to the formation of silicon nitride and silicon oxynitride on the surface. NO^+ ion dissociates on impact with Si target and produces energetic N and O atoms. The N and O atoms reacts with Si surface to form silicon oxide and silicon nitride. Further bombardment leads to oxidation and nitridation of silicon nitride and silicon oxide, respectively, and forms silicon oxynitride [36]. Generally, the rate of nitridation of silicon oxide is more than the rate of oxidation of silicon nitride and hence silicon nitride exists with silicon oxynitride. Previously, it was reported by our group that off normal incidence of NO^+ ion on Si surface forms silicon oxide and silicon oxynitride at different parts of nanostructure[18,19]. Similarly, in case of ($CO^+ + N_2^+$) ion bombardment, the simultaneous reaction of carbon, nitrogen and oxygen leads to silicon carbide, silicon oxide and silicon nitride formation at the early stage. With further bombardment, the silicon nitride and a part of silicon oxide react to form more stable oxynitride (found in broad peak) [18,19].

In order to investigate the modification of the thin layer with depth,

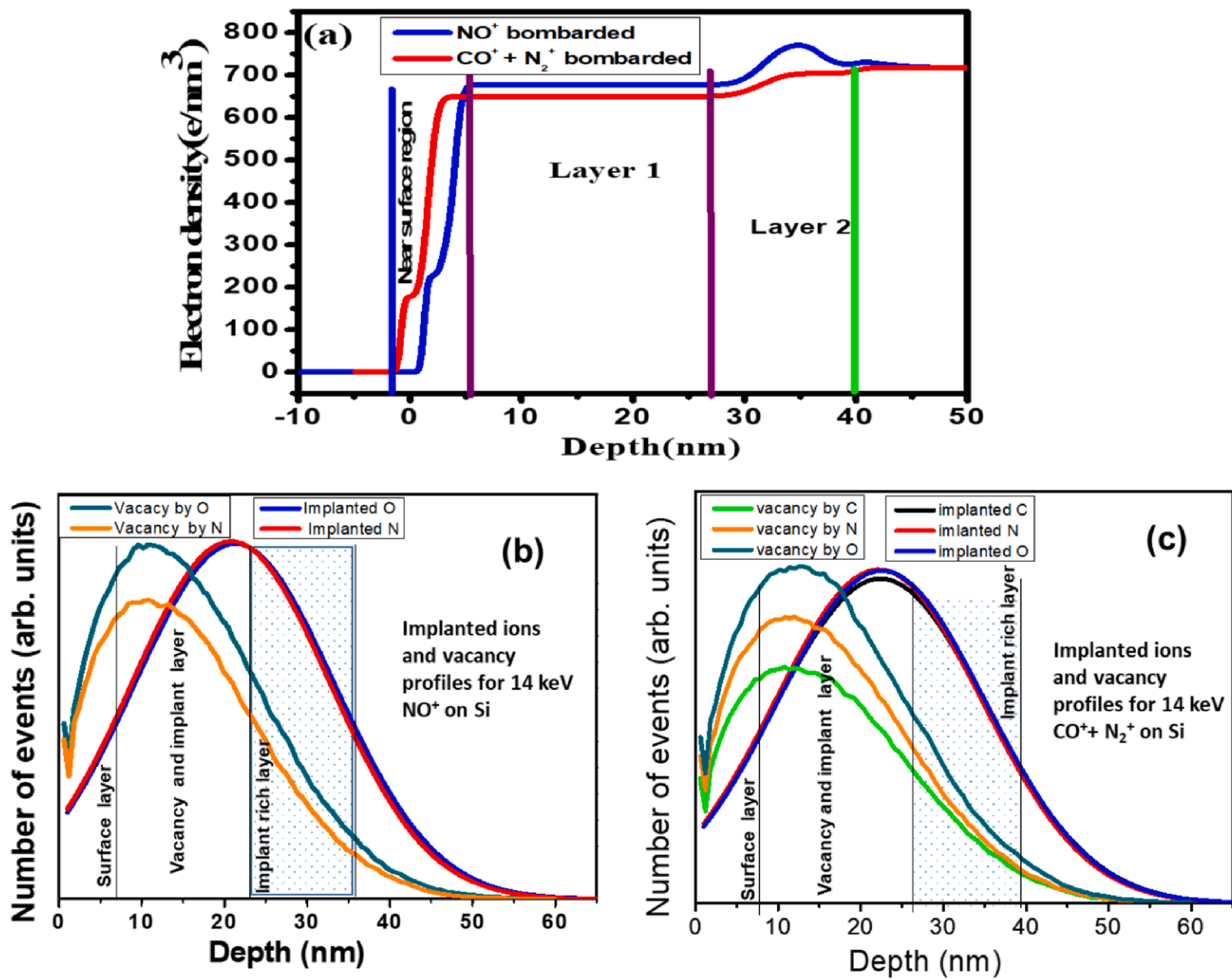

Fig. 5. (a) Electron density profile as a function of depth obtained from X-ray Reflectivity measurements. Monte Carlo (SRIM) simulation for the estimation of vacancy and the implant rich regions due to (b) NO^+ and (c) ($CO^+ + N_2^+$) ion bombardment on Si.

X-ray reflectivity measurements as a function of q_z (=4π Sin θ/λ) for virgin and ion modified Si samples are presented in Fig. 4. The REFLEX program is used to fit experimental data and this program is based on transfer matrix method calculation [37 38]. Interaction with electromagnetic radiation of a material can be described using complex refractive index. The refractive index of the jth medium of a material is given by $\eta_j = 1 - \delta_j - i\beta_j$, where δ_j is related to atomic scattering factor and electron density and β_j is related to the x-ray absorption[37]. During fitting, each film is modelled with several layers and each of these layers consists of four parameters: *δ, β,* thickness and interface roughness. The parameters are optimized using Nelder-Mead Simplex algorithm [39]. The Chi-square (χ^2) parameter, which is used to describe the match between calculated profile and experimental data, is given by.

$$\chi^2 = \frac{1}{n}\sum_{i=1}^{n}\left(\frac{I^i_{data} - I^i_{cal}}{I^i_{data}}\right)^2$$

where, n is total data points. I^i_{data} and I^i_{cal} are the experimental and calculated values of ith data point. The electron density values are extracted from these optimized parameters. Significant changes in the calculated curve and in Chi-square are found if these parameters differ by ± 2% from its optimized values.

Reflectivity spectrum of virgin Si (Fig. 4 (a)) contains no oscillation. The presence of hump (or oscillation) in reflectivity spectra of ion modified surfaces (Fig. 4(b) and (c)) clearly indicates modified film/layer formation [40]. The rapid fall of reflectivity at $q_z = 0.1$ nm^{-1} indicates the damping of the oscillation due to high roughness at surface and interface of the film [41,42].. The obtained electron density profile (EDP) is shown inset of each figure. The EDP of virgin Si indicates the presence of native oxide layer of thickness ~ 1.5 nm and then a constant electron density is found around 700 for the bulk Si. On the other hand, the electron density profile has multiple steps near the surface region for NO^+ and ($CO^+ + N_2^+$) ion bombarded Si. It indicates multiple chemical phase formation near the surface (around 5 nm) for molecular or ($CO^+ + N_2^+$) ion bombardment as observed from XPS measurement. At deeper depth, between 5 and 25 nm, the electron density remains almost constant for both the cases. A dip and hump of thickness ~ 12 nm is observed for both the cases in the depth range 25 to 37 nm. During ion bombardment, Si atoms are knocked and displaced, which results in vacancy formation. Also, the projectile ions are implanted at a certain depth of Si substrate without having reaction with Si atoms [43] leading to increase in electron density. These effects are responsible for the variation of electron density profile.

To estimate the damage layer as well as the profile of the implanted ions in Si substrate, Monte Carlo simulation is carried out using SRIM (BCA) software [20]. We assume that NO^+ and ($CO^+ + N_2^+$) ions dissociate on impact and the energy sharing follows the energy and linear momentum conservation. Therefore, 14 keV NO^+ is equivalent to 6.47 keV N^+ and 7.53 keV O^+, while 14 keV ($CO^+ + N_2^+$) ion is equivalent to 6 keV C^+, 7 keV N^+ and 8 keV O^+. The estimation of vacancy and implantation profiles by the projectiles are presented in Fig. 5 (b) and (c). It is observed that vacancy profile is extended from the surface to 40 nm deep with the peak around 12 nm and FWHM of 25 nm. The depth

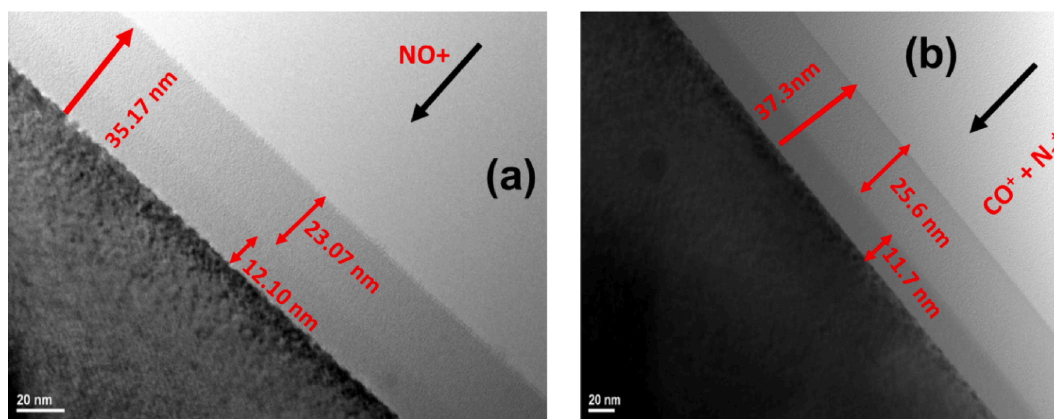

Fig. 6. Cross sectional TEM study of (a) NO^+ (b) (CO^+ $+N_2^+$) ion bombarded Si;

profile of implanted species is shifted by 12 nm compared to the vacancy profile and has the peak at 25 nm. Thus, an amorphous layer of about 40 nm is expected while the implanted species are mostly populated at the end part of the modified layer.

Therefore, it is clear from X-ray reflectivity measurements that NO^+ and (CO^++ N_2^+) ion bombardment leads to form a modified thin layer, which can be subdivided into three sub layers. However, the interfaces between the layers are not sharp, which is also evident from the electron density profile and SRIM calculation (Fig. 5). The topmost ultrathin layer (~5 nm) is enriched with different chemical phases (oxide, nitride, oxynitride and carbide) due to the direct chemical reaction of top surface atoms with the reactive projectiles. In case of NO^+ bombarded Si, the topmost layer consists of a mixture of silicon nitride and oxynitride, whereas in case of (CO^+ + N_2^+) ion bombardment, the top surface is the mixture of silicon carbide, silicon oxynitride and silicon oxide. The electron densities of silicon compounds are lower comparative to pure-Si. The electron density profile near the surface (upto ~ 5 nm) (Fig. 5a) and XPS data (Fig. 2 &3) of the surface, thus, support the formation of different chemical phases of Si near the surface after NO^+ and (CO^+ + N_2^+) ion bombardment.

Fig. 7. (a)-(b) study of Optical response by UV-IR spectroscopy (c)-(d) estimation of refractive index of virgin and ion bombarded Si surfaces.

The next layer (layer 2) is mainly amorphous silicon having ion induced vacancies and implanted ions. This layer of approximate thickness 15–20 nm shows almost constant electron density from the XRR measurements (Fig. 4). SRIM [20] calculation have identified this region (Fig. 5) where both Si vacancies and implant species are present. This layer is mainly enriched with Si vacancies, but also have certain number of implanted species. The third layer (approx. from 25 nm to 40 nm) consists more amount of the implanted ions than the vacancies where the electron density profile shows a dip and hump (Figs. 4 and 5 (a)). It is found from the SRIM [20] calculation that the projectile ions will be mostly implanted at a depth of around 25 nm and extended upto 50 nm. The implanted ion profiles are also shifted right by approx. 12 nm compared to the vacancy profile. Thus, the developed third layer is also amorphous silicon but enriched with implanted projectile ions.

In order to visualize the three parts in the reactive ion modified thin layer, high-resolution Transmission Electron Microscopy (HRTEM) study is carried out and presented in Fig. 6. The topmost chemically modified layer is not distinguishable from the TEM data, but vacancy rich amorphous layer (second layer) and implanted ion rich third layer in both the cases are clearly visible. In the case of NO^+ bombardment, two amorphous layers with thickness 23.07 nm and 12.10 nm are formed. Similarly, in case of (CO^+ + N_2^+) ion bombardment, two amorphous thin layers of 25.6 nm and 11.7 nm thickness are formed. Shift of the implantation profile by approximately 12 nm than the vacancy profile (SRIM calculation in Fig. 5) leads to form implant rich amorphous third layer of approximate thickness 10–12 nm. Therefore, the cross-sectional TEM study also shows a good agreement with XRR data and Monte Carlo simulation.

Energetic ions of NO^+ and (CO^++N_2^+) transfers their energy to the target atoms and forms a collision cascades. Vacancy and interstitial defects (Frenkel pair) are formed in the target and the projectile ions are implanted at a depth (range) where energy becomes nearly zero. Thus, a damage layer is formed up to the range of projectile ion and the projectile ions are implanted throughout the damaged layer. The damages and implants are non-uniformly distributed as a function of depth. The peak of the vacancy distribution is always at a lower depth than the peak of ion range distribution [44,45]. Fig. 5 show the distribution profile of vacancies and implanted ions, respectively, for NO^+ (Fig. 5b) and (CO + N_2^+) (Fig. 5b) ion bombardment on Si using the SRIM freeware [20]. Ion surface interaction simulation, in static condition, by SRIM freeware cannot describe exactly the implantation and damage profile as observed experimentally, but it gives an indication that a vacancy rich and an implant rich regions may form in the present case. The first sub-layer at the surface is developed due to the differential sputtering of Si and its compounds. The ion-modified layer consists of amorphous silicon atoms and compounds of silicon as described above. For continue ion bombardment with projectile ions the damage creation and implantation occurs inside the Si, simultaneously, surface atoms are sputtered and the surface boundary shifts towards the depth. Due to preferential sputtering of Si, the surface layer becomes different from the rest of the modified layer. The sputtering of Si is always more when it is in pure form than its compounds (oxide, carbide, nitride, oxynitride) during the impact of C, N and O ions [46]. Continue bombardment leads to enrich the surface layer by the compounds of Si than pure Si. Thus, the surface layer (first sub-layer) of approximately 5 nm thick is formed as detected by XRR electron density profile (Fig. 5a).

The optical sensitivity of virgin and ion modified Si layer is investigated by UV–VIS-IR reflectance spectroscopy for wavelength range 200 nm to 1200 nm. The penetration depth of the UV–VIS-IR light depends on its wavelength. Generally, the penetration of the UV light in silicon is very less compared to visible light [47]. The change in reflectivity occurs due to change in surface chemical nature, amorphization on the surface, defect/damage formation, multiple layer formation on the substrate. The polished virgin Si surface exhibits a maximum reflectance of 75% in UV region (near 300 nm), as shown in Fig. 7(a). The spectra contain three peaks at 217 nm (5.7 eV), 274 nm (4.5 eV) and 368 nm (3.36 eV) in UV region. Similar peaks were also observed by Schmidt et. al [48] and the spectra resemble to that reported by Liu et al. [49]. It is clear from Fig. 7(a) that virgin Si is more sensitive to EM wave at lower wavelength region (UV region) compared to visible region. The well-known fact that the bandgap of virgin Si lies in IR region (around 1127 nm) and hence the reflectivity decreases at this wavelength as observed here. The presence of multiple layers with silicon oxide, nitride, oxynitride, carbide in the top surface, changes the reflectivity of the UV-IR spectra. The reflectivity of NO^+ and (CO^+ + N_2^+) ion bombarded Si surfaces reduces drastically in UV region as observed in Fig. 6(b). The variation of reflectance spectra of NO^+ bombarded Si resembles with the reflectance spectra of silicon nitride in lower wavelength region, whereas in higher wavelength region, the spectra is similar to the spectra of silicon oxide [50,51]. Compared to silicon nitride and oxide, silicon carbide is a wide bandgap material with high absorbance. The presence of sufficient amount of silicon carbide (Table 1) in case of (CO^+ +N_2^+) ion bombarded Si lowers the reflectivity in UV region compared to NO^+ bombarded Si. Therefore, in our case, the presence of multiple chemical phases on the top surface layers lead to lowering the reflectivity of the Si surfaces in UV region compared to virgin Si. The UV–Vis data is used to estimate the variation of absorption coefficient with photon wavelength. The absorption co-efficient is estimated by Kubelka Munk's method. In case of reflectance spectra, the absorption coefficient (α) is related to reflectivity by the equation $\alpha = (1\text{-R})^2 / 2\text{R}$, where R is the reflectivity. This technique relates the Tauc's plot with Kubelka-Munk's plot. The absorption edge is defined as the point beyond which a sharp rise in absorbance is found. The ion bombardment causes a shift in absorption edge from 280 nm (virgin Si) to 240 nm (NO^+) bombarded Si (inset of Fig. 7(a) and (b)). This indicates the good optical property of the fabricated ultrathin films [52].

To investigate the change in dielectric property of these ultrathin films, the variation of refractive index with photon energy is presented in Fig. 7(c) & (d). The refractive index is directly related to dielectric property of the material. In between the several methods of estimating the refractive index, the spectrophotometry method is used to estimate the refractive index of the ion modified surface. The reflectivity (*R*) is related to the refractive index by the relation $n = \frac{(1+R)}{(1-R)} + \left\{\frac{4R}{(1-R)^2} - K^2\right\}$, [53] where *R* is the reflectivity and *K* is the extinction or attenuation coefficient. The attenuation coefficient is defined as $K = \alpha\lambda/4\pi$, where α is the absorption coefficient and λ is the photon wavelength. This method is known as Hapke's method [63], which is applicable for diffused reflection spectroscopy (DRS) of thin films as well as powder samples [55]. A nonlinear variation of refractive index is seen for virgin and ion modified Si surfaces (Fig. 7(c)&(d)). Similar kind of spectra for virgin Si is already reported by El-Sayed et.al [54]. Generally, all these chemical phases are well known dielectric and possess a nonlinear refractive index which is evident from Fig. 7(d). The refractive index of NO^+ bombarded Si surface is maximum at 500 nm and minimum at 250 nm (Fig. 7(d)). On the other hand, the variation of refractive index of (CO^+ + N_2^+) ion bombardment is much less compared to NO^+ bombarded case (Fig. 7(d)). Refractive index is also UV sensitive. This can be considered as a resonant effect, which occurs between incident light photons and electronic polarization of the sample. The equality between the plasma frequency and the incident photon led to electron coupling in the oscillating electric field in UV region, hence the peaks are observed [55].

The change in optical band gap due to change in surface chemical nature is estimated using Kubelka-Munk's theory [56]. Multiple linear portions of the equation $[\text{F(R)}h\nu]^{1/n} = \text{B}\,(h\nu - \text{E}_g)$, are extrapolated in energy axis (from inflection point where $\frac{d(F(R)h\upsilon)^2}{d(h\upsilon)} = 0$) to determine the optical bandgap of the material. We consider $n = 2$ and ½ for direct and indirect transitions, respectively. E_g is the optical bandgap and *B* is a constant [57]. The corresponding reflectivity (*R*) data of virgin and ion modified surfaces are used to calculate Kubelka-Munk's function,

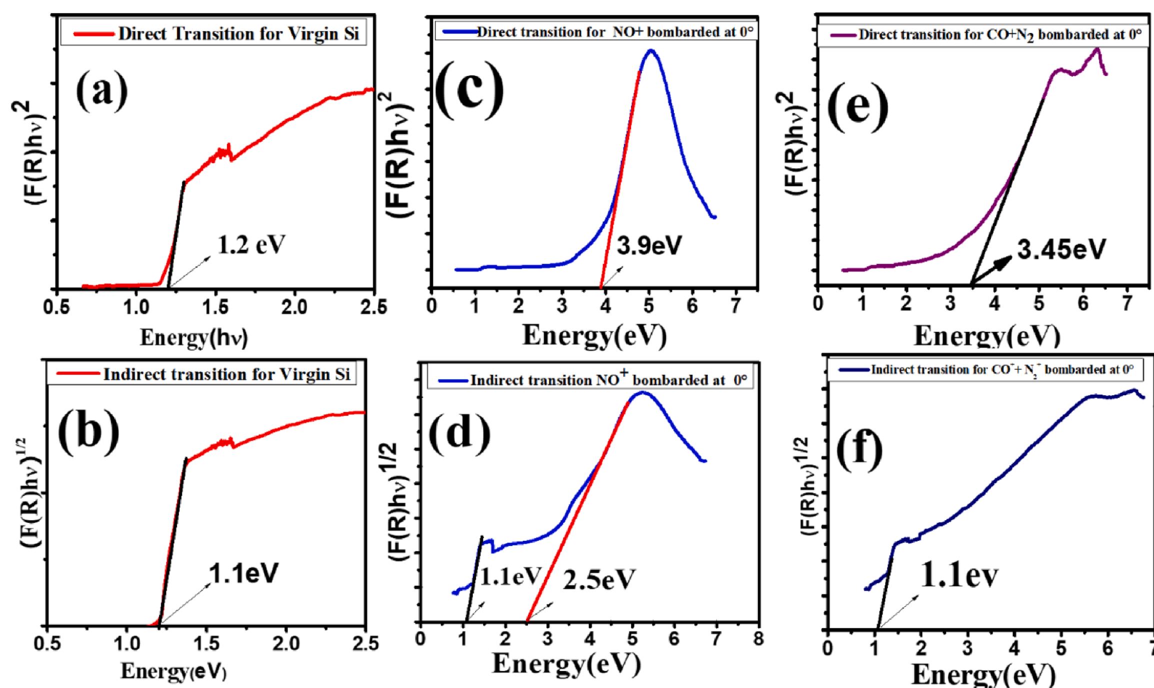

Fig. 8. Estimation of direct and indirect optical bandgap of (a) & (b) virgin and (c)-(f) ion bombarded Si surfaces.

Table 2
Estimated bandgap of virgin Si and ion modified ultrathin films on Si surface.

Sample	Direct bandgaps (eV)	Indirect bandgaps (eV)
Virgin Si	*1.2*	*1.1*
NO^+ bombarded Si	*3.9*	*2.5*
$CO^+ + N_2^+$ ion bombarded Si	*3.45*	*No bandgap in UV-IR region*

defined as $F(R) = \frac{(1-R)^2}{2R}$. The optical bandgap of virgin Si in both direct and indirect modes are presented here in Fig. 8(a) and (b). It is well known that optical bandgap of virgin Si is 1.2 eV and 1.1 eV in direct and indirect mode, respectively [58]. The ion induced modification changes the bandgap as shown in Fig. 8 (c)-(f). The NO^+ bombarded Si surface (which is a mixture of silicon nitride and silicon oxynitride) exhibits two direct bandgaps of 3.9 eV and an indirect bandgap of 2.5 eV as seen in Fig. 8(c) and (d), respectively. The ($CO^+ + N_2^+$) ion bombardment Si surface (having a mixture of four chemical phases) shows a single direct bandgap of 3.45 eV but no indirect bandgap is found in this region except the bandgap of Si (Fig. 8 (e) & (f)). Interestingly, in each indirect transition, the band gap of Si (an indirect bandgap semiconductor with a bandgap of 1.1 eV) is present. [59]. The estimated bandgap of virgin and ion modified Si surfaces are listed in Table 2. The bandgap of silicon oxide, nitride and carbide are 8.9 eV, 5.1 eV, and 3.26 eV [60]. Nevertheless, the mixture of amorphous silicon oxide, oxynitride, nitride and carbide indicate a lowering of the bandgap. However, the bandgap of silicon oxynitride generally varies from 2 eV to 4 eV depending upon the stoichiometric ratio of oxygen and nitrogen [60]. Hence, the bandgap observed in these cases, are due to major contribution of silicon oxynitride.

4. Conclusions

In conclusion, we have studied ultrathin layer formation on Si surface by nitric oxide and ($CO^+ + N_2^+$) ion irradiation. The ultra-thin film formation with more than one chemical phase can be achieved by irradiating the Si surface with these ion beam. The irradiation of these two beams leads to simultaneous irradiation of carbon, nitrogen and oxygen like reactive ions on Si surface. The simultaneous reaction of carbon, nitrogen and oxygen with silicon atoms leads to form multiple chemical phases. The presence of multiple chemical phases and bandgap can be used for tailoring the optical absorption and reflection from the surface, which is important for electromagnetic shielding, anti-reflection coating, biological applications etc. The presence of silicon carbide, silicon oxynitride and silicon oxide leads to a variation of dielectric property applicable for different optical fiber, graded index fiber, gate dielectrics in optoelectronic devices etc. [61,62]. Moreover, the tailoring of bandgap over a wide range indicates its uses in photovoltaic device, solar cell applications while implanted rich layer is formed at a depth of 25 to 37 nm followed by an intermediate amorphous Si layer of 20 nm thickness.

CRediT authorship contribution statement

Joy Mukherjee: Methodology, Validation, Visualization, Investigation, Formal analysis, Software, Writing – original draft. **Sudip Bhowmick:** Investigation. **Sabyasachi Karmakar:** Investigation, Formal analysis. **Dipak Bhowmik:** Formal analysis. **Biswarup Satpati:** Investigation, Formal analysis. **Satyajit Hazra:** Visualization. **Prasanta Karmakar:** Conceptualization, Methodology, Investigation, Validation, Visualization, Formal analysis, Writing – review & editing, Supervision.

Declaration of Competing Interest

The authors declare that they have no known competing financial interests or personal relationships that could have appeared to influence the work reported in this paper.

Data availability

Data will be made available on request.

References

[1] L. Jiang, R. Cheung, A review of silicon carbide development in MEMS applications, Int. J. Comput. Mater. Sci. Surf. Eng. 2 (2009) 227.

[2] T. Zhang, S.-R. Zhang, M.-Q. Wu, W.-J. Sang, Z.-P. Gao, Z.-P. Li, Studies on dielectric properties of silicon nitride at high temperature, J. Elec. Sci. Technol. China 5 (2007) 316–319.
[3] A.E. Kaloyeros, Y. Pan, J. Goff, B. Arkles, Review—silicon nitride and silicon nitride-rich thin film technologies: state-of-the-art processing technologies, properties, and applications, ECS J. Solid State Sci. Technol. 9 (2020), 063006.
[4] D.T.H. Tan, K.J.A. Ooi, D.K. Tng, Nonlinear optics on silicon-rich nitride—a high nonlinear figure of merit CMOS platform, Photonic research 6 (2018) B50.
[5] N. Vidakis, M. Petousis, E. Velidakis, L. Tzounis, N. Mountakis, A. Korlos, P. E. Fischer-Griffiths, S. Grammatikos, On the Mechanical Response of Silicon Dioxide Nanofiller Concentration on Fused Filament Fabrication 3D Printed Isotactic Polypropylene Nanocomposites, Polymers 13 (2021) 2029.
[6] Y. Wu, Y.-M. Lee, The Performance and Reliability of PMOSFET's with Ultrathin Silicon Nitride/Oxide Stacked Gate Dielectrics with Nitrided Si-SiO2 Interfaces Prepared by Remote Plasma Enhanced CVD and Post-Deposition Rapid Thermal Annealing, IEEE Trans. Electron Devices 47 (2000) 1361–1369.
[7] T. Storgaard-Larsen, O. Leistiko, Plasma-Enhanced Chemical Vapor Deposited Silicon Oxpitride Films for Optical Waveguide Bridges for Use in Mechanical Sensors, J. Electrochem. Soc 144 (1997) 1505–1513.
[8] D. Zhou, L. Huang, J. Yuan, C. Li, Influences of different sputtering current on the microstructure and electrical properties of silicon nitride thin films deposited on cemented carbide tools, Ceramic Int. 47 (2021) 32160–32167.
[9] I. Ferain, C.A. Colinge, J.-P. Colinge, Multigate transistors as the future of classical metal oxide semiconductor field effect transistors, Nature 479 (2011) 310–316.
[10] A. Agarwal, H.-J. Gossmann, D.J. Eaglesham, L. Pelaz, S.B. Herner, D.C. Jacobson, T.E. Haynes, R. Simonton, Damage, defects and diffusion fromultra-low energy 0 up to 5 kev ion implantation of silicon., Materials Science in Semiconductor Processing, 1 (1998) 17-25.
[11] S. Dauwe, L. Mittelstaedt, A. Metz, R. Hezel, Experimental evidence of parasitic shunting in silicon nitride rear surface passivated solar cells, Prog. Photovolt. Res. Appl. 10 (2002) 271–278.
[12] S. Fischer, Ultra Thin Silicon Nitride Interface Engineering, in: Elektrotechnik und Informationstechnik, Rheinisch-Westfälischen Technischen Hochschule Aachen, 2017.
[13] J.M. Maloney, S.A. Lipka, S.P. Baldwin, In Vivo Biostability of CVD Silicon Oxide and Silicon Nitride Films, Mater. Res. Soc. Symp. Proc 872 (2005) J14.13.11.
[14] E. Ermakova, Y. Rumyantsev, A. Shugurov, A. Panin, M. Kosinova, PECVD synthesis, optical and mechanical properties of silicon carbon nitride films, App. Surf. Sci 339 (2015) 102–108.
[15] V.P. Popov, V.A. Antonov, L.N. Safronov, I.N. Kupriyanov, Y.N. Pal'yanov, S. Rubanov, Fabrication of ultra-thin diamond films using hydrogen implantation and Liftoff technique, Aip Conference Proceedings, 1496 (2012) 261.
[16] D. Bhowmik, S. Bhattacharjee, D. Lavanyakumar, V. Naik, B. Satpati, P. Karmakar, Synthesis of nano-patterned and Nickel Silicide embedded amorphous Si thin layer by ion implantation for higher efficiency solar devices, App. Surf. Sci 422 (2017) 11–16.
[17] I.A. Kurzina, E.V. Kozlov, Y.P. Sharkeev, A.I. Ryabchikov, I.B. Stepanov, I.A. Bozhko, M.P. Kalashnikov, D.O.S. c, S.V. Fortuna, Influence of ion implantation on nanoscale intermetallic-phase formation in Ti–Al, Ni–Al and Ni–Ti systems, Surface & Coatings Technology, 201 (2007) 8463–8468.
[18] J. Mukherjee, D. Bhowmik, M. Mukherjee, B. Satpati, P. Karmakar, Alternating silicon oxy-nitride and silicon oxide stripe formation by nitric oxide (NO+) ion implantation, J. Appl.Phys 127 (2020), 145302.
[19] J. Mukherjee, D. Bhowmik, G. Bhattacharyya, B. Satpati, P. Karmakar, Spatially varying chemical phase formation on silicon nano ripple by low energy mixed ions bombardment, J. Phys:Conds.Matt 34 (2022), 135001.
[20] J.F. Ziegler, M.D. Ziegler, J.P. Biersack, Srim –,, The stopping and range of ions in matter, Nucl. Instrum. Method Sect.B 268 (2010) 1818–1823.
[21] S. Mandal, M. Mukherjee, S. Hazra, Evolution of Electronic Structures of Polar Phthalocyanine-Substrate Interfaces, ACS Appl. Mater. Interfaces 12 (2020) 45564–45573.
[22] F. De, H. Feng, X. Junlin, X. Lihui, Calibration of Binding Energy Positions with C1s for XPS Results, Journal of Wuhan University of Technology-Mater, Sci. Ed. 35 (2020) 711–718.
[23] K. Levenberg, A Method for The solution Of cetain of Non Linear Problems in Least Square, Q Appl. Math 2 (1944) 164–168.
[24] S. Roy, M. Saifuddin, S. Mandal, S. Hazra, Stearic acid mediated growth of edge-on oriented bilayer poly (3-hexylthiophene) Langmuir films, J. Colloid Interface Sci. 606 (2022) 1153–1162.
[25] S.S.Chao, Y.Takagi, G.Lucovsky, P.PaiR.C.Custer, J.E.Tyler, J.E.Keem, Chemical states study of Si in SiOx films grown by PECVD, Appl. Surf. Sci., 26 (1986) 575.
[26] M. Delfino, J.A. Fair, S. Salimian, Thermal nitridation of silicon in a cluster tool, Appl. Phys. Lett 60 (1992) 341.
[27] R.v. Weeren, E.A. Leone, S. Curran, L.C. Klein, S.C.D. ', Synthesis and Characterization of Amorphous Si,N,O, J. Am.Cer. Soc., 77 (1994) 2699-2702.
[28] T. Parrill, Y.W. Chung, Surface analysis of cubic silicon carbide, Surf. Sci. 243 (1991) 96–112.
[29] F. Rueda, J. Mendialdua, A. Rodriguez, R. Casanova, Y. Barbaux, L. Gengembre, L. Jalowiecki, Characterization of Venezuelan laterites by X-ray photoelectron spectroscopy, J. Elec. Spec. Rel. Phen 82 (1996) 135–143.
[30] D. Sprenger, H. Bach, W. Meisel, P. Gi~tlich, XPS study of leached glass surfaces, J. Non-Crystalline Solid, 126 (1990) 111-129.
[31] L. Bois, P. L'Haridon, Y. Laurenta, X. Gouinb, P. Grangeb, J.-F. Lktard, M. Birot, J.-P. Pillot, J. Dunogub, Characterization of a boro-silicon oxynitride prepared by thermal nitridation of a polyborosiloxane, J. Alloys. Comp. 232 (1996) 244–253.
[32] T.A. Clarke, E.N. Rizkalla, X-ray photoelectron spectroscopy of some silicates, Chem. Phys. Lett. 37 (1976) 523.
[33] C. Guimon, D. Gonbeau, G. Pfister-Guillouzo, O. Dugne, A. Guette, R. Naslain, M. Lahaye, XPS Study of BN Thin Films Deposited by CVD on Sic Plane Substrates, Suf. Interf. Anal. 16 (1990) 440–445.
[34] J.A. Taylor, G.M. Lancaster, J.W. Rabalais, Chemical Reaction of N2 ion beams with group IV elements and their oxides, J. Elec. Spec. Rel. Phen 13 (1978) 435–444.
[35] K.L. Smith, K.M. Black, Characterization of the treated surfaces of silicon alloyed pyrolytic carbon and SiC, J. Vac. Sci. Technol. A 2 (1984) 744.
[36] C. Jimenez, J. Perri6re, I. Vickridge, J.P. Enard, J.M. Albella, Transformation of silicon nitride in oxygen plasma, Surface & Coatings Technology, 45 (1991) 147-154.
[37] A. Gibaud, G. Vignaud, Specular Reflectivity from Smooth and Rough Surfaces. , in: J. Daillant, A. Gibaud (Eds.) X-ray and Neutron Reflectivity. Lecture Notes in Physics, Springer Berlin, Heidelberg, 2009.
[38] G. Vignaud, A. Gibaud, REFLEX: a program for the analysis of specular X-ray and neutron reflectivity data, J. Appl. Cryst. 52 (2019) 201–213.
[39] F. Gao, L. Han, Implementing the Nelder-Mead simplex algorithm with adaptive parameters, Comput Optim Appl 51 (2012) 259–277.
[40] S. Kundu, S. Hazra, S. Banerjee, M.K. Sanyal, S.K. Mandal, S. Chaudhuri, A.K. Pal, Morphology of thin silver film grown by dc sputtering on Si(001), J.Phys.D: Applied Physics, 31 (1998) L73-L77.
[41] R. Krawietz, B. Wehner, D. Meyer, K. Richter, H. Mai, R. Dietsch, S. Hopfe, R. Scholz, W. Pompe, Investigation of the thermal stability of Ni/C multilayers by X-ray methods, Fresenius J Anal Chem 353 (1995) 246–250.
[42] M.K. Sanyal, A. Datta, S. Banerjee, A.K. Srivastava, B.M. Arora, S. Kanakaraju, S. Mohan, X-ray Reflectivity Study of Semiconductor Interfaces, J. Synchrotron Rad 4 (1997) 185–190.
[43] S.O. Kucheyeva, J.E. Bradby, C.P. Li, S. Ruffell, T.v. Buuren, T.E. Felter, Effects of carbon on ion-implantation-induced disorder in GaN, App.Phys.Lett, 91 (2007) 261905.
[44] W. Möller, Fundamentals of ion-solid interac.
[45] J.P. Biersack, Three-dimensional distributions of ion range and damage including recoil transport, Nucl. Inst. Methods Phys. Res. B 19 (20) (1987) 32–39.
[46] J. Mukherjee, D. Bhowmik, M. Mukherjee, B. Satpati, P. Karmakar, Alternating silicon oxy-nitride and silicon oxide stripe formation by nitric oxide (NO+) ion implantation, J. Appl.Phys 127 (2020).
[47] Y.R.S.C.d. Silva, R. Kuroda, S. Sugawa, A Highly Robust Silicon Ultraviolet Selective Radiation Sensor Using Dierential Spectral Response Method, Sensors, 19 (2019).
[48] J.A. Schmidt, N. Budini, P. Rinaldi, R.D. Arce, R.H. Buitrago, Nickel-induced crystallization of amorphous silicon, XIX Latin American Symposium on Solid State Physics 167 (2009), 012046.
[49] Y. Liu, G. Ji, J. Wang, X. Liang, Z. Zuo, Y. Shi, Fabrication and photocatalytic properties of silicon nanowires by metal-assisted chemical etching: effect of H2O2 concentration, Nanoscale Res. Lett. 7 (2012) 663.
[50] P. Hlubina, J. Lunacek, D. Ciprian, R. Chlebus, Spectral interferometry and reflectometry used to measure thin films, Applied physics, B. Lasers and Optics 92 (2008) 203–207.
[51] K. Jhansirani, R.S. Dubey, M.A. More, S. Singh, Deposition of silicon nitride films using chemical vapor deposition for photovoltaic applications, Results Phys. 6 (2016) 1059–1063.
[52] A.A. Akl, H. Kamal, K. Abdel-Hady, Fabrication and characterization of sputtered titanium dioxide films, App. Surf. Sci 252 (2006) 8651–8656.
[53] M.M. El-Nahass, H.S. Soliman, A. El-Denglawey, Absorption edge shift, optical conductivity, and energy loss function of nano thermal-evaporated N-type anatase TiO2 films, Appl. Phys. A 122 (2016) 775.
[54] E.-S.Y. El-Zaiat, GamalM.Youssef, Dispersive parameters for complex refractive index of p-and n-type silicon from spectrophotometric measurements in spectral range200–2500nm, Optics&LaserTechnology, 65 (2015) 106-112.
[55] A.S. Hassanien, A.A. Akl, Optical characteristics of iron oxide thin films prepared by spray pyrolysis technique at different substrate temperatures, Appl. Phys. A 124 (2018) 752.
[56] L. Yang, B. Kruse, R. Kubelka-Munk theory, I. Theory and application, J. Opt. Soc. Am. A 21 (2004) 1933–1941.
[57] G.D. Gesesse, A. Gomis-Berenguer, M.-F. Barthe, C.O. Ania, On the analysis of diffuse reflectance measurements to estimate the optical properties of amorphous porous carbons and semiconductor/carbon catalysts, J. Photochem. & Photobio., A: Chem. 398 (2020), 112622.
[58] A.R. Zanatta, Revisiting the optical bandgap of semiconductors and the proposal of a unifed methodology to its determination, Sci. Rep. 9 (2019) 11225–112236.
[59] P. Makula, M. Pacia, W. Macyk, How To Correctly Determine the Band Gap Energy of Modified Semiconductor Photocatalysts Based on UV-Vis Spectra, J. Phys. Chem. Lett. 9 (2018) 6814–6817.
[60] V.A. Gritsenko, N.D. Dikovskaja, K.P. Mogilnikov, Band diagram and conductivity of silicon oxynitride films, Thin Solid Films 51 (1978) 353–357.
[61] J. Bauer, Optical Properties, Band Gap, and Surface Roughness of Si, N, Phys. stat. sol. (a) 39 (1977) 411.
[62] A.E. amrani, I. Menous, L. Mahiou, R. Tadjine, A. Touati, A. Lefgoum, Silicon nitride film for solar cells, Renewable Energy, 33 (2008) 2289–2293.
[63] Huafeng Huang, Diane M. Colabello, Elizabeth C. Sklute, Timothy D. Glotch and Peter G. Khalifah, Self-Referenced Method for Estimating Refractive Index and Absolute Absorption of Loose Semiconductor Powders, *Chem. Mater.* 29 (2017) 4632–4640.